

Cite as: J. Vac. Sci. Technol. B **39**, 053203 (2021); https://doi.org/10.1116/6.0001205 Submitted: 08 June 2021 • Accepted: 29 July 2021 • Published Online: 30 August 2021

Chengwu Zhang, Tuo Gao, Donal Sheets, et al.

COLLECTIONS

æ

This paper was selected as an Editor's Pick







ARTICLES YOU MAY BE INTERESTED IN

Modeling the initial monolayer formation in thermally localized surface deposition Journal of Vacuum Science & Technology B **39**, 052802 (2021); https://doi.org/10.1116/6.0001098

Selective dry etching of UV-nanoimprinted resin passivation masks for area selective atomic layer deposition of aluminum oxide

Journal of Vacuum Science & Technology B **39**, 052804 (2021); https://doi.org/10.1116/6.0001250

Next generation nanopatterning using small molecule inhibitors for area-selective atomic layer deposition

Journal of Vacuum Science & Technology A **39**, 021002 (2021); https://doi.org/10.1116/6.0000840







Cite as: J. Vac. Sci. Technol. B **39**, 053203 (2021); doi: 10.1116/6.0001205 Submitted: 8 June 2021 · Accepted: 29 July 2021 · Published Online: 30 August 2021







Chengwu Zhang,^{1,2} Tuo Gao,^{1,2} Donal Sheets,^{2,3} Dason N. Hancock,^{2,3} Jason Tresback,⁴ and Brian Willis^{1,2,a)}

AFFILIATIONS

- Department of Chemical and Biomolecular Engineering, University of Connecticut, Storrs, Connecticut 06269
- ²Institute of Materials Science, University of Connecticut, Storrs, Connecticut 06269
- ³Department of Physics, University of Connecticut, Storrs, Connecticut 06269
- ⁴Center for Nanoscale Systems, Harvard University, Cambridge, Massachusetts 02138

ABSTRACT

Nanogaps in metallic nanostructures produce local field enhancements with potential applications in surface enhanced spectroscopy, solar energy conversion, and photocatalysis. Atomic layer deposition is applied as a conformal coating to modify nanogap sizes and tune the optical properties of plasmonic dimer arrays with sub-10 nm nanogaps. Nanostructures are fabricated using layers of gold and palladium to combine features of plasmonics and area-selective atomic layer deposition, where copper metal is deposited on palladium-covered surfaces. Direct measurements of optical extinction for successive smaller nanogaps and thicker copper coatings show that spectral features become broadened at first due to heating-induced shape changes but subsequently sharpen as copper coatings form on palladium structures. Furthermore, longitudinal resonances of plasmonic dimers blue shift for thin coatings due to heating and decreasing aspect ratio, but thicker coatings lead to red shifts due to narrowing nanogaps. Together, these results show that area-selective atomic layer deposition is a promising tool for achieving large area arrays of plasmonic dimers with sub-10 nm nanogaps.

Published under an exclusive license by the AVS. https://doi.org/10.1116/6.0001205

I. INTRODUCTION

Plasmonic dimers, especially with sub-10 nm nanogaps, can greatly enhance local electric field intensity through excitations of surface plasmons, which are collective oscillations of electrons excited by light.^{1,2} Arrays of plasmonic dimers made of materials such as copper, silver, and gold can be designed to concentrate and manipulate light at the nanoscale, and they have wide applications in areas such as surface enhanced spectroscopy, photo-driven chemical conversion, and photodetection.^{1,3,4} These applications benefit from intense electric fields, hot carriers produced by surface plasmon decay, or laser-induced plasmonic local heating.^{3–5} Nanogaps between plasmonic dimers create electric field hot spots that grow more intense as the gap is reduced, reaching electric field enhancements as large as 10³.⁶

Previous studies to fabricate plasmonic dimers with sub-10 nm nanogaps include techniques such as electromigration, 6-8 electroless

gold plating, ^{9,10} self-assembly, ¹¹ and high resolution electron beam lithography. ^{12–18} However, these methods are limited in shape and pattern design, or low yield for scaling up. Moreover, the methods generally do not allow for tunability of nanogap dimensions. To attain more flexibility and reliability in fabrication, there is a need for scalable methods to fabricate plasmonic dimers with sub-10 nm nanogaps, which is crucial for their use in practical applications.

Atomic layer deposition (ALD) is a thin-film deposition technique capable of producing conformal thin films with precise control of thickness and composition at the atomic level. 19,20 Area-selective ALD (AS-ALD) is a bottom-up process for direct deposition of materials only on desired regions of a substrate. 21–24 Our previous work shows how AS-ALD can be used to tune plasmonic responses. 25,26 It provides a flexible and reliable way to tune nanogaps to modify optical and electrical properties. In this approach, arrays of palladium dimer nanostructures are fabricated

a)Electronic mail: brian.willis@uconn.edu

as templates, and copper AS-ALD is applied to tune nanogaps and enhance plasmonic properties. Palladium acts as a nucleation layer to enable copper ALD growth on nanostructures.^{25–28}

In this work, we investigate copper AS-ALD to tune nanogaps of plasmonic dimer arrays to sub-10 nm. Nanostructure templates are made of layered Au/Pd to enhance plasmonic properties. Optical responses are compared before and after deposition to analyze the effects of copper coatings on plasmonic properties.

II. EXPERIMENT

Gold (Au), palladium (Pd), and layered Au/Pd plasmonic dimer arrays were fabricated on fused quartz substrates by highresolution electron beam lithography, electron beam evaporation, and lift-off processing. Schematic diagrams of the fabrication process are shown in Fig. S1 of the supplementary material.³⁹ The array sizes are $200 \times 200 \,\mu\text{m}^2$ and the square unit cells are 550 nm in both planar directions. The sizes of the nanorods are $(130 \pm 3) \times (43 \pm 1) \text{ nm}^2$ and tuned to a resonance near 800 nm. A thin layer of 4 nm titanium was used to promote adhesion to the fused quartz substrate. For reference experiments, 40 nm thick pure gold or pure palladium was subsequently deposited onto the titanium layer. For ALD experiments, dimer templates were made of Au/Pd; 36 nm Au was deposited on the titanium layer, followed by 10 nm of Pd. After fabrication, wafers were protected with photoresist and diced into $1 \times 1 \text{ cm}^2$ die. Before optical measurements, each die was rinsed with acetone to remove photoresist, cleaned by isopropyl alcohol, and dried with nitrogen gas.

Optical extinction of the arrays was measured using a polarized transmission experimental setup, which is based on our previous work. 26,29 To measure optical extinction, we first measure the transmission of the substrate as a background signal. Next, the array of interest is moved to the focused beam spot. Subsequently, polarized transmission of each array is measured and optical extinction is given by $1-T_{\rm array}/T_{\rm sub}$, where $T_{\rm array}$ is the transmission of the array and $T_{\rm sub}$ is the transmission for the substrate. Full width at half maximum (FWHM) was calculated by fitting a Lorentzian curve to extinction peaks and measuring the width at half maximum.

Prior to ALD growth experiments, each die was pretreated to clean and activate surfaces. After photoresist removal, each sample was treated with an oxygen plasma to remove surface contaminants and subsequently dipped in dilute hydrofluoric acid (250:1 $\rm H_2O:49\%~HF)$ to remove the top few layers of the quartz substrate. Finally, samples were dried with nitrogen gas and further cleaned by ultraviolet-ozone for 10 min. Samples were then immediately loaded into the ALD reactor.

ALD growth experiments were done in a custom-built tool, which is shown schematically in Fig. 1. Samples were placed onto a pedestal-style sample holder, which is heated by an embedded cartridge heater with an integral thermocouple. The external surfaces of the reactor were heated by tungsten-halogen bulbs to 125 °C to prevent precursor condensation. Temperatures were regulated by a proportional, integral, derivative controller. Sample temperatures were calibrated by thermocouple measurements on the heat stage. A custom-built heating vaporizer and heat tapes

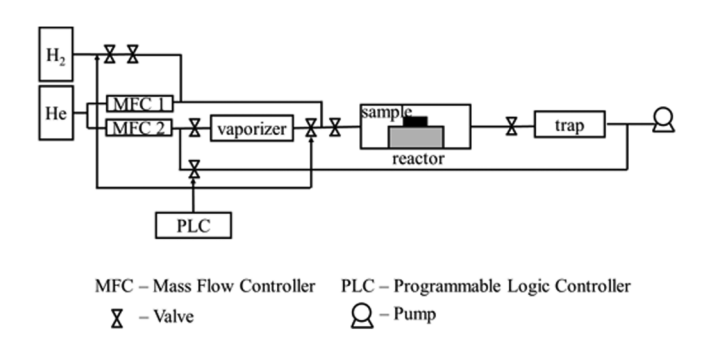


FIG. 1. Schematic diagram of a custom-fabricated ALD tool.

were used to maintain a controlled heated path from the precursor source to the reactor. Helium was used as a delivery and purge gas to minimize temperature oscillations during hydrogen pulsing. Flow rates of carrier and purge gases were controlled by mass flow controllers and set at 20 and 144 SCCM, respectively, which corresponded to reactor pressure at 1 Torr. Copper bis-(2, 2, 6, 6-tetramethyl-3, 5-heptanedionate) [Cu (thd)₂] and hydrogen act as precursor and co-reactant, respectively, for this AS-ALD reaction. The precursor was ground to a fine powder and heated to 120 °C to sublimate. The ALD temperature window for this AS-ALD reaction is from 190 to 260 °C. All depositions in this study were done at 230 °C to ensure a high growth rate while maintaining good selectivity.³⁰ The partial pressure of hydrogen gas was tuned to 1 Torr by a needle valve. ALD valves were controlled by a programmable logic controller for pulsing of copper precursor and hydrogen. ALD pulsing times for hydrogen dosing, helium purge, copper precursor dosing, and helium purge were set as 2, 3, 3, and 3s, respectively.

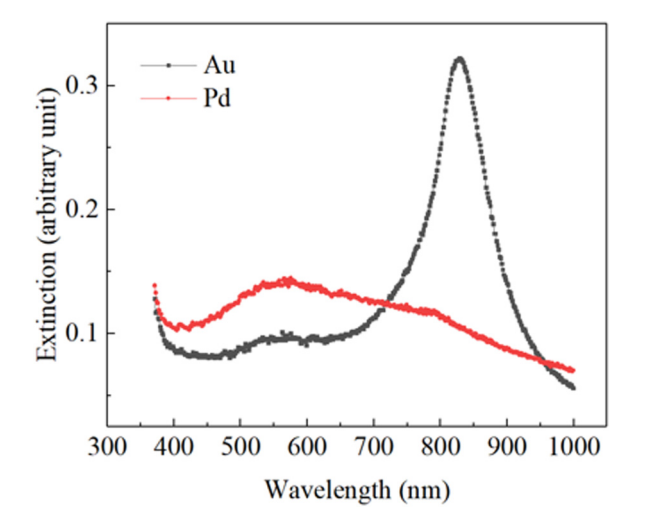


FIG. 2. Extinction curves of $200 \times 200 \, \mu \text{m}^2$ Au and Pd dimer nanostructure arrays.

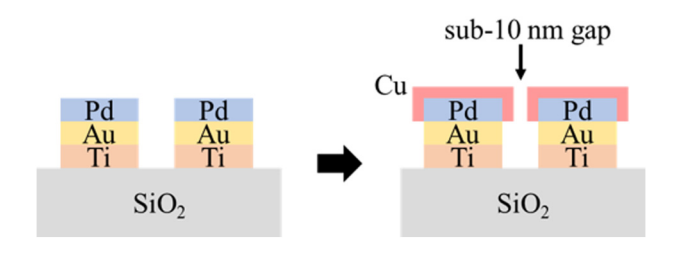


FIG. 3. Side view schematic diagram of AS-ALD to tune nanogaps (not to scale).

After ALD growth experiments, samples were analyzed by high-resolution scanning electron microscopy (SEM) to quantify structure sizes and nanogaps. Before SEM imaging, samples were sputter coated with a 2 nm layer of gold for charge dissipation. A Verios SEM was used with an accelerating voltage of 10 kV and a beam current of 0.4 nA, which gives a resolution of 0.9 nm. Image magnification was set at 150 000x, and immersion mode was used for high-resolution imaging. The quantification analysis of images was done using ProSEM software (GenISys GmbH). All the structure sizes and nanogaps in each image were measured, and the averaged data are given in Figs. 7(c) and 7(b). Samples were analyzed by a Cypher atomic force microscope (AFM) to extract the height profiles of plasmonic dimer arrays. Imaging was performed in noncontact, AC/tapping mode in air using soft (2 N/m) cantilevers with a 7:1 aspect ratio silicon tip. The average height in each sample is given in Fig. 7(d).

III. RESULTS AND DISCUSSION

As a reference for growth experiments, the extinction curves for gold and palladium dimer nanostructures were measured and

compared. Figure 2 shows extinction curves for gold and palladium dimer nanostructure arrays of the same nominal size and thickness. The electric field polarization is along the dimer axis. The gold arrays show one sharp peak around 830 nm with a FWHM of 86.2 ± 1.7 nm, indicating a strong dipolar plasmon resonance. In contrast, palladium dimer nanostructure arrays have two broad peaks centered near 560 and 800 nm. The weak extinction of palladium is mostly due to its inferior plasmonic properties but may also be attenuated by oxidation or carbonaceous layers caused by sample preparation and air exposure. The small peak in the palladium spectrum near 800 nm was consistent over many samples and is assigned to a weak dipolar resonance.

Based on the weak plasmonic properties of palladium compared to gold, we fabricated Au/Pd-layered templates as a compromise between the good nucleation properties of palladium and the good plasmonic properties of gold. Copper AS-ALD was then applied to investigate the optical properties as nanogaps are reduced to sub-10 nm. Figure 3 shows a side view diagram of the layer design for ALD growth. Gold layers provide strong plasmonic resonances in the visible and near IR range, and palladium layers promote copper nucleation.^{25–28} Using copper AS-ALD, nanogaps could be precisely and reproducibly tuned below 10 nm.

Figure 4(a) shows a top-down SEM image of a Au/Pd-layered dimer nanostructure array prior to ALD growth. These are nanofabricated templates for ALD growth. The gap size distribution is shown in Fig. S2. The average size of all nanogaps (20 in total) is 11.9 ± 1.6 nm, and the nanorod size is $(130 \pm 3) \times (43 \pm 1)$ nm². For the selected example in Fig. 4(b), edges of the nanorods are well defined by ProSEM software. The gap sizes are quantified by using edge detection algorithms and analyzing pixel intensity.

Growth experiments using 50, 100, and 200 cycles of copper AS-ALD were used to narrow the nanogaps fabricated from the templates. Figure 5(a) displays a top-down SEM image of a Au/Pd-layered dimer nanostructure array after 200 cycles copper AS-ALD at 230 °C. Compared with SEM images prior to ALD

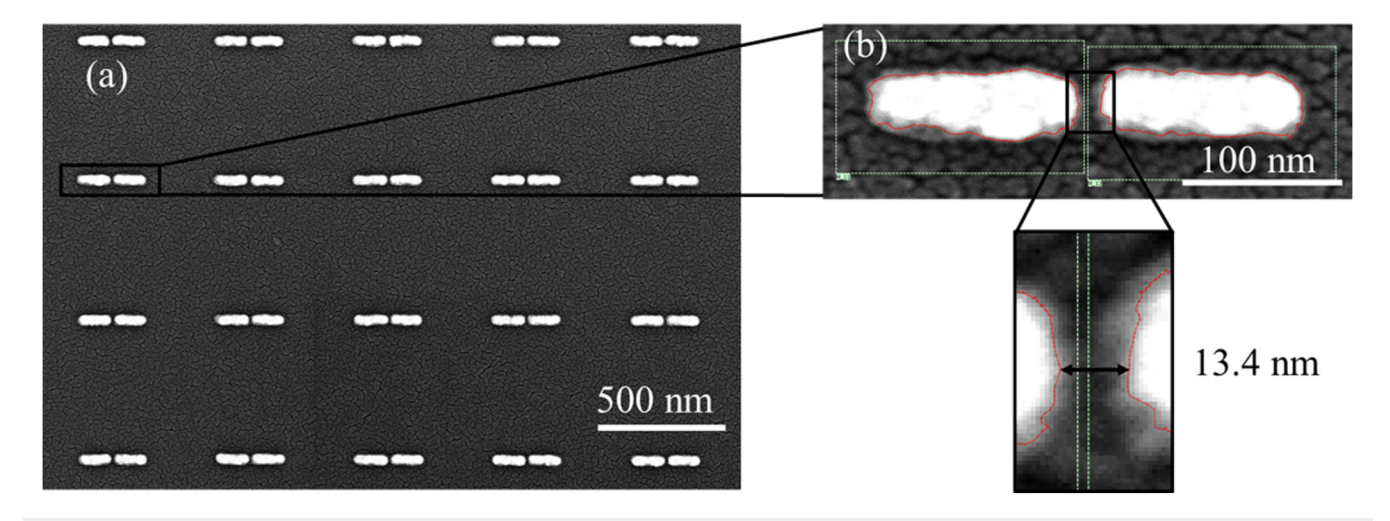


FIG. 4. (a) Top-down SEM image of a Au/Pd-layered dimer nanostructure array prior to ALD growth; (b) example of dimer nanostructure dimension measurements by ProSEM.

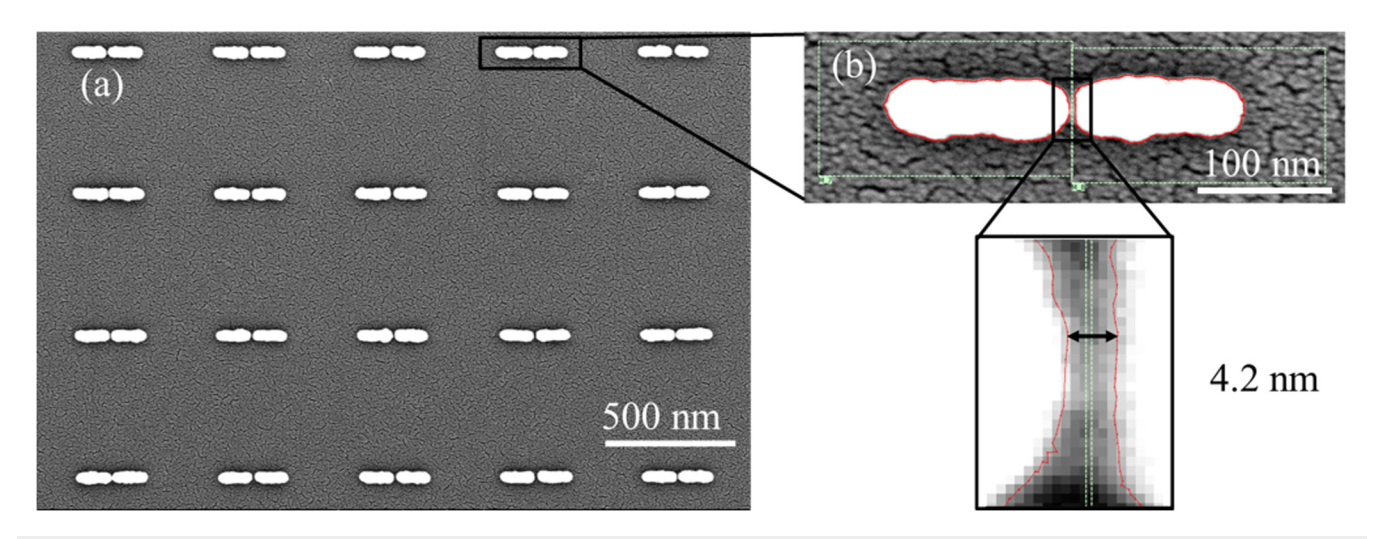


FIG. 5. (a) Top-down SEM image of a Au/Pd-layered dimer nanostructure array after 200 cycles of copper AS-ALD at 230 °C; (b) example of dimer nanostructure dimension measurements by ProSEM.

growth, dimer nanostructures in post-ALD samples become larger and more rounded, while the substrate surfaces remain clear of metal deposits. Only a charge dissipation layer is present on the substrate surface, which confirms the selective growth. The gap size distribution is shown in Fig. S2. The average size of all nanogaps (20 in total) is 6.5 ± 2.2 nm. The nanogap of the example in Fig. 5(b) is 4.2 nm based on the ProSEM analysis. In the inset, each pixel is 0.9 nm and this nanogap is around 4–5 pixels. Thus, AS-ALD demonstrates reliable tunability in nanogaps from 11.9 ± 1.6 to 6.5 ± 2.2 nm. The deposition is conformal as evidenced by growth in the length and width of the features. The slight increase in standard deviation from 1.6 to 2.2 nm is consistently observed across many samples and patterns. Smaller nanogaps are achieved with more ALD growth, but nanogaps become difficult to quantify below 5 nm.

Optical extinction curves were measured to track the changes of plasmonic resonances in the AS-ALD process. Figure 6 shows extinction measurements for light polarized along the axis of the dimer nanostructures. The extinction curve of Au/Pd-layered templates prior to growth (black curve) is significantly broader than the gold extinction curve in Fig. 2, with a FWHM of 157.6 ± 1.6 nm. This is caused by the damping effect of palladium thin layers.³¹ In the first 50 cycles of deposition, the extinction curve (red curve) becomes slightly broader with a FWHM of 165.6 ± 8 nm. This peak broadening is primarily due to heating, which can also be seen in Fig. S3 (Ref. 39) for control experiments with heating but no ALD growth. During subsequent copper deposition, FWHM decreases to 141 ± 5 nm after 100 ALD cycles (blue curve) and further to 140 ± 3 nm after 200 cycles (green curve), which is narrower than the starting Au/Pd templates. The curves gradually sharpen as copper continuously coats the palladium structures because copper has similar plasmonic properties as gold, which is of higher quality than palladium at optical frequencies.³¹, There may also be a contribution to the reduction in peak width

due to the red shift of the resonance. Intuitively, experiments show that reducing the palladium layer thickness results in higher quality resonances. However, a sufficient palladium layer is necessary to nucleate and sustain copper ALD growth. ^{25–28}

As shown in Fig. 6, the resonance peak position initially blue shifts around 100 nm after 50 ALD cycles and then red shifts back after more deposition cycles. The initial blue shift is mainly due to heat-induced rounding of corners and edges, which is driven by thermodynamics to minimize surface energy. ^{26,35} Control experiments with heating but without growth in Fig. S3 (Ref. 39) show similar blue shifts. ³⁹ Figures S4(a) and S4(b) ³⁹ show 3D

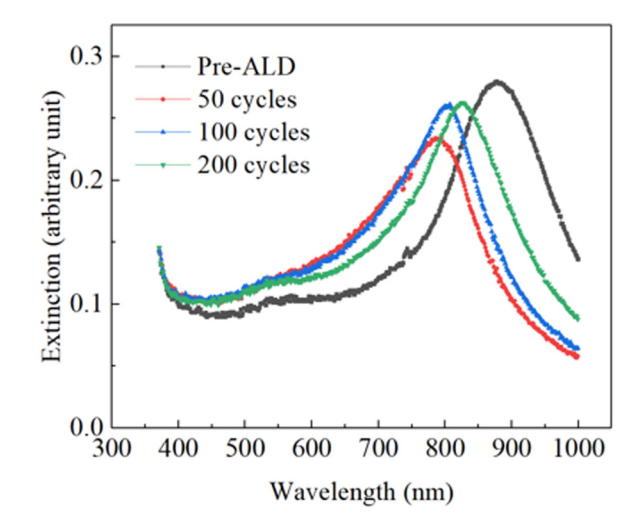


FIG. 6. Extinction curves of Au/Pd-layered dimer nanostructure arrays after copper AS-ALD for 50, 100, and 200 cycles of growth.

high-resolution AFM images of Au/Pd dimer nanostructure arrays prior to ALD growth.³⁹ Initially, the edges of dimer nanostructures are sharp and the top surfaces are rough. However, features become significantly rounded and smoother after 50 cycles of growth, which is displayed in Fig. S4(c).³⁹ The heat-induced rounding effect is also seen in SEM images. Further rounding and smoothing are seen after 100 and 200 cycles in Figs. S4(d) and S4(e),³⁹ which are also shown by the height line scanning results in Fig. S5.³⁹

Additional factors that affect the optical properties include a decreasing aspect ratio from 3.0 ± 0.1 to 2.7 ± 0.1 [Fig. 7(a)], which also contributes to a blue shift of the resonance. The initial sharp decline and gradual saturation of the aspect ratio is consistent with conformal coatings. Uniform coatings on nanorods naturally lead to a reduction of the aspect ratio, where rectangular features become less elongated with increasing deposition layers. Additional data in Figs. 7(c) and 7(d) show larger growth in the width and height directions compared to the length direction, which is

consistently observed across many samples and patterns. After 200 ALD cycles, the average growth in the length direction is 5.6 nm, while growth in the width direction is 7.7 nm and growth in the height direction is 7.4 nm. The growth difference is caused by thermodynamically driven reduction of surface energy that tends to blunt sharp features and round corners. Lower temperatures or different deposition chemistries may improve the AS-ALD approach by maintaining higher aspect ratios or by reducing the need for palladium seed layers. 36,37

After initial blue shifts from heating and growth, the resonance peak red shifts because of the reduction in the nanogaps. 13,16,26,29,38 As displayed in Fig. 7(b), average nanogaps decrease from 11.9 \pm 1.6 to 6.5 \pm 2.2 nm after 200 cycles of growth. The reduction is roughly linear with the number of cycles. The red shifts are caused by hybridization of the nanorod plasmons, which reduces the restoring force and decreases the resonant frequency. 13,29,31 For fixed nanorod sizes, reducing nanogaps can lead

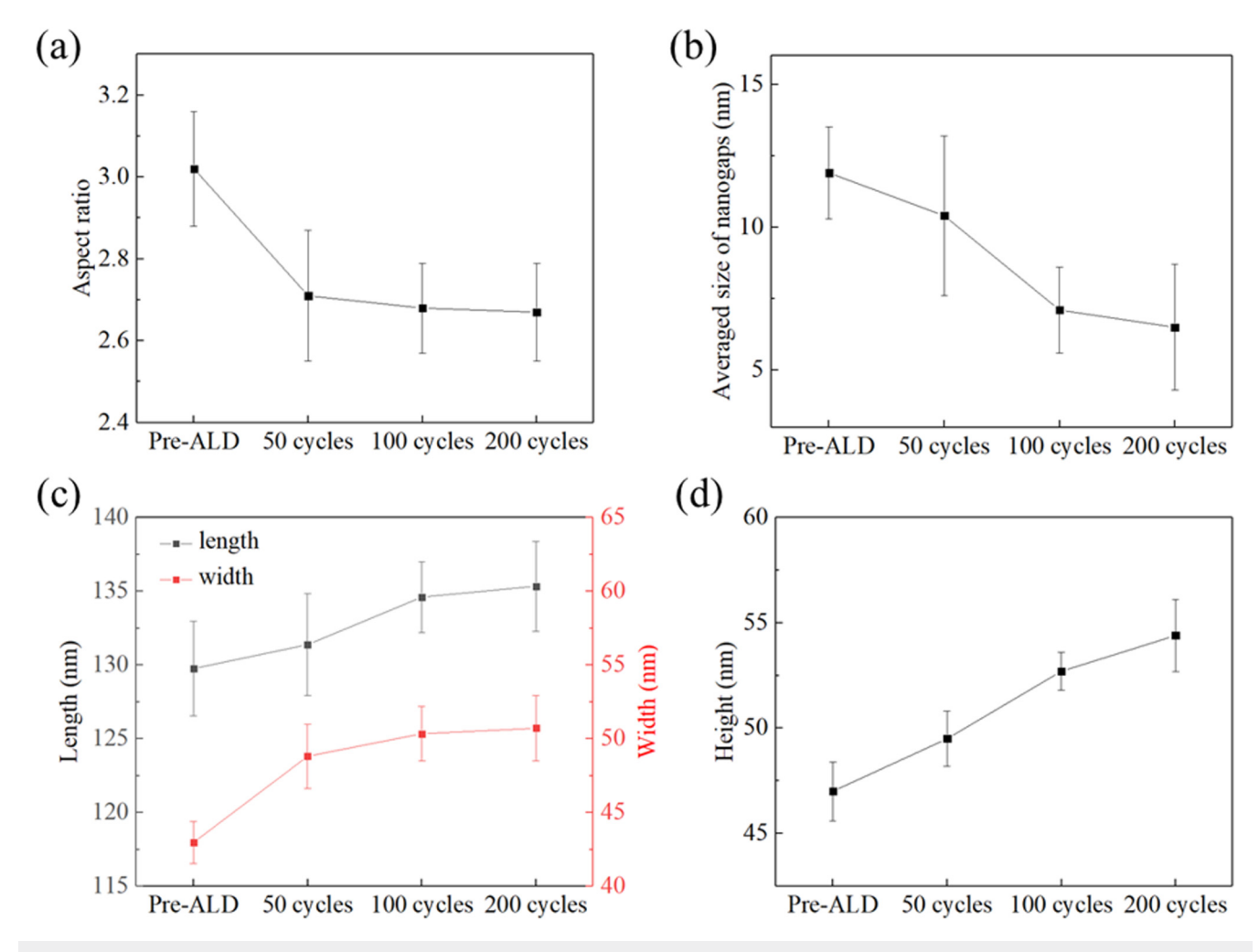


FIG. 7. Dimension changes in the AS-ALD process: (a) aspect ratio, (b) size of nanogaps, (c) length and width of nanorods, and (d) height of nanorods.



to significant red shifts, especially when gap sizes are below 10 nm. The red shifts observed in Fig. 6 from 50 to 200 cycles are relatively small at 41 nm. The reasons for the small shifts are that nanogap reductions are accompanied by offsetting factors associated with ALD growth that include decreased aspect ratio and increased height.

IV. CONCLUSIONS

We present a tunable and scalable method to fabricate plasmonic dimer arrays with sub-10 nm nanogaps using AS-ALD. Sizes of nanogaps were imaged by high-resolution SEM measurements and quantified by ProSEM software. Extinction curves of plasmonic dimer arrays were collected by a broadband source in a confocal transmission arrangement. The extinction curves of Au/Pd-layered templates prior to growth are significantly broader than pure gold due to the damping effects of palladium layers. During growth, extinction curves initially blue shift due to heating and decreasing aspect ratio and become slightly broader. In contrast, thicker coatings lead to red shifts due to the dominant effect of narrowing nanogaps. Extinction features gradually sharpen as copper coats the palladium layers and improves the resonances. AS-ALD provides a reliable way to tune the optical properties of plasmonic dimers and achieve sub-10 nm nanogaps on large area arrays.

ACKNOWLEDGMENTS

The authors acknowledge the National Science Foundation (NSF) (Grant Nos. 1511138, ECCS-2025158, and NSF-DMR-1905862), the Office of Naval Research (Grant No. N00014-19-1-2246), the Department of Energy (Grant No. DE-SC0016481), and a Thermo Fisher Scientific Fellowship for support. Nanofabrication and AFM were performed at the Harvard University Center for Nanoscale Systems (CNS). SEM was performed at the UConn/Thermo Fisher Scientific Center for advanced Microscopy and Materials Analysis (CAMMA).

DATA AVAILABILITY

The data that support the findings of this study are available within the article and its supplementary material.

REFERENCES

- ¹J. A. Schuller, E. S. Barnard, W. Cai, Y. C. Jun, J. S. White, and M. L. Brongersma, Nat. Mater. **9**, 193 (2010).
- ²J. G. Smith, J. A. Faucheaux, and P. K. Jain, Nano Today **10**, 67 (2015).
- ³E. Cortes, W. Xie, J. Cambiasso, A. S. Jermyn, R. Sundararaman, P. Narang, S. Schlucker, and S. A. Maier, Nat. Commun. **8**, 14880 (2017).
- ⁴S. Linic, P. Christopher, and D. B. Ingram, Nat. Mater. 10, 911 (2011).
- ⁵M. L. Brongersma, N. J. Halas, and P. Nordlander, Nat. Nanotechnol. **10**, 25 (2015).
- ⁶D. R. Ward, F. Huser, F. Pauly, J. C. Cuevas, and D. Natelson, Nat. Nanotechnol. 5, 732 (2010).
- ⁷D. R. Ward, N. K. Grady, C. S. Levin, N. J. Halas, Y. Wu, P. Nordlander, and D. Natelson, Nano Lett. 7, 1396 (2007).

- ⁸H. Park, A. K. Lim, A. P. Alivisatos, J. Park, and P. L. McEuen, Appl. Phys. Lett 75,301 (1999).
- ⁹V. V. Serdio, Y. Azuma, S. Takeshita, T. Muraki, T. Teranishi, and Y. Majima, Nanoscale 4, 7161 (2012).
- ¹⁰V. M. Serdio V, T. Muraki, S. Takeshita, D. E. Hurtado, S. Kano, T. Teranishi, and Y. Majima, RSC Adv. 5, 22160 (2015).
- ¹¹J. Kern et al., Nano Lett. **12**, 5504 (2012).
- ¹²L. Dong et al., Nano Lett. **17**, 5768 (2017).
- ¹³W. Zhu, M. G. Banaee, D. Wang, Y. Chu, and K. B. Crozier, Small 7, 1761 (2011)
- ¹⁴A. Fursina, S. Lee, R. G. S. Sofin, I. V. Shvets, and D. Natelson, Appl. Phys. Lett. **92**, 113102 (2008).
- ¹⁵A. L. Koh, D. W. McComb, S. A. Maier, H. Y. Low, and a. J. K. W. Yang, J. Vac. Sci. Technol. B 28, C6O45 (2010).
- 16H. Hu, H. Duan, K. Kumar, Z. Shen, and J. K. W. Yang, ACS Nano 5, 7593 (2011).
- 17 A. L. Koh, A. I. Fernandez-Dominguez, D. W. McComb, S. A. Maier, and J. K. Yang, Nano Lett. 11, 1323 (2011).
- ¹⁸H. Duan, A. I. Fernandez-Dominguez, M. Bosman, S. A. Maier, and J. K. Yang, Nano Lett. **12**, 1683 (2012).
- ¹⁹S. M. George, Chem. Rev. **110**, 111 (2010).
- ²⁰R. W. Johnson, Adam Hultqvist, and S. F. Bent, Mater. Today 17, 236 (2014).
- ²¹H.-B.-R. Lee and S. F. Bent, Chem. Mater. 32, 3323 (2020).
- ²²M. Fang and J. C. Ho, ACS Nano 9, 8651 (2015).
- ²³G. N. Parsons and R. D. Clark, Chem. Mater. 32, 4920 (2020).
- ²⁴A. J. M. Mackus, A. A. Bol, and W. M. M. Kessels, Nanoscale 6, 10941 (2014).
- ²⁵R. A. Wambold, P. H. Cutler, N. M. Miskovskyd, J. Qie, G. J. Weisel, B. G. Willis, and D. T. Zimmerman, Plasmonics: Metallic Nanostructures and Their Optical Properties XIII, San Diego, California, United States (28 August, 2015), Vol. 9547, p. 95471H.
- ²⁶R. A. Wambold, B. D. Borst, J. Qi, G. J. Weisel, B. G. Willis, and D. T. Zimmerman, Nanophotonics 10, 026024 (2016).
- ²⁷X. Jiang, H. Wang, J. Qi, and B. G. Willis, J. Vac. Sci. Technol. A 32, 041513 (2014).
- ²⁸J. Qi, D. T. Zimmerman, G. J. Weisel, and B. G. Willis, J. Chem. Phys. **147**, 154702 (2017).
- ²⁹D. T. Zimmerman, B. D. Borst, C. J. Carrick, J. M. Lent, R. A. Wambold, G. J. Weisel, and B. G. Willis, J. Appl. Phys. 123, 063101 (2018).
- 30 P. Martensson and J.-O. Carlsson, J. Electrochem. Soc. 145, 2926 (1998).
- ³¹F. A. Nugroho, B. Iandolo, J. B. Wagner, and C. Langhammer, ACS Nano 10, 2871 (2016).
- ³²M. D. Huntington, A. Yang, M. F. Cardinal, S. S. Masango, R. P. Van Duyne, and Teri W. Odom, ACS Nano 8, 7639 (2014).
- ³³D. Manchon et al., Nanoscale 7, 1181 (2015).
- ³⁴R. Pilot, R. Signorini, C. Durante, L. Orian, M. Bhamidipati, and L. Fabris, Biosensors (Basel) 9, 57 (2019).
- 35 J.-H. Song, T. Atay, and A. V. Nurmikko, Nano Lett. 4, 1627 (2004).
- 36P. G. Gordon, A. Kurek, and S. T. Barry, ECS J. Solid State Sci. Technol. 4, N3188 (2015).
- ³⁷T. J. Knisley, L. C. Kalutarage, and C. H. Winter, Coord. Chem. Rev. 257, 3222 (2013).
- 38 P. K. Jain, W. Huang, and a. M. A. El-Sayed, Nano Lett. 7, 2080 (2007).
- 39 See supplementary material at https://www.scitation.org/doi/suppl/10.1116/6.0001205 for schematic diagrams of the sample fabrication process, gap size distributions before and after ALD, extinction curves in a control experiment, AFM images of nanostructures before and after ALD, and height line scanning of nanostructures.